Characterization of the grape powdery mildew genetic resistance loci in *Muscadinia rotundifolia* Trayshed

Mélanie Massonnet, Amanda M. Vondras, Noé Cochetel, Summaira Riaz, Dániel Pap, Andrea Minio, Rosa Figueroa-Balderas, M. Andrew Walker, Dario Cantu*

Department of Viticulture and Enology, University of California Davis, Davis, CA 95616, USA

*Corresponding author:
dacantu@ucdavis.edu

Abstract

Muscadinia rotundifolia cv. Trayshed is a valuable source of resistance to grape powdery mildew (PM). It carries two PM resistance (*R*) loci, *Run1.2* on chromosome 12 and *Run2.2* on chromosome 18. This study identified the nucleotide-binding leucine-rich repeat (NLR) genes composing each *R* locus and their associated defense mechanisms. Evaluation of PM disease development showed that introgression of both loci confers resistance to PM in a *V. vinifera* background, but with varying speed and intensity of the response. To better understand the effect of NLR composition on PM resistance, both haplotypes of each *R* locus were reconstructed and the gene models within each haplotype were manually refined. We found that the number and classes of NLR genes differed between *Run1.2* and *Run2.2* loci and between the haplotypes of each *R* locus. In addition, NLR genes composing *Run1.2b* or *Run2.2* loci exhibited different levels of gene expression, pointing to candidate NLR genes responsible for PM resistance in Trayshed. Finally, a transcriptomic analysis that included six additional *R* loci showed differences in the defense mechanisms associated with *Run1.2b* and *Run2.2* in response to PM and at constitutive level. Altogether, our results reveal that Trayshed's *R* loci are composed of distinct NLRs that trigger different plant defense mechanisms in response to PM and at constitutive level, which would explain the variation of pathogen restriction between the two loci.

Introduction

Grapevine powdery mildew (PM) is a devastating fungal disease caused by *Erysiphe necator* Schwein. (syn. *Uncinula necator*), an obligate biotrophic ascomycete that can infect all green organs of a grapevine (Gadoury *et al*., 2012). Cultivated grapevines that belong to *Vitis vinifera* (ssp. *vinifera*) are highly susceptible to PM. Fungicide sprays are applied prophylactically to control the disease but are costly (Sambucci *et al*., 2019). Natural resistance to PM exists in several wild grapes. Thirteen PM resistance-associated loci were identified in the last two decades (Dry *et al*., 2019; Karn *et al*., 2021). *Vitis* includes several PM-resistant species, including *V. romanetii* (Ramming *et al*., 2010; Riaz *et al*., 2011) and *V. piasezkii* (Pap *et al*., 2016), which are native to China, *V. vinifera* ssp. *sylvestris* from Central Asia (Riaz *et al*., 2020), the North American *V. cinerea* (Dalbó e*t al.*, 2001), and the muscadine grape, *Muscadinia rotundifolia* (Pauquet e*t al.*, 2001; Feechan e*t al.*, 2013; Riaz e*t al.*, 2011).

Muscadinia rotundifolia is closely related to *Vitis* (Small, 1913) and is resistant to several diseases in addition to PM (Olmo, 1971; Olmo, 1986), including downy mildew (*Plasmopara viticola*), Pierce's disease (*Xylella fastidiosa*), and phylloxera (*Daktulosphaira vitifolia*). Two major loci associated with PM resistance were found in *M. rotundifolia*. *Resistance to Uncinula necator 1* (*Run1*), located on chromosome 12, and its alternative form, *Run1.2*, were identified in *M. rotundifolia* G52 and Trayshed, respectively (Pauquet *et al*. 2001; Riaz *et al*., 2011). *Run2.1* and *Run2.2* were identified on chromosome 18 of *M. rotundifolia* Magnolia and Trayshed, respectively (Riaz *et al*., 2011). Both haplotypes of Trayshed's *Run1.2* were associated with PM resistance and designated *Run1.2a* and *Run1.2b* (Feechan *et al*., 2013).

M. rotundifolia is an ideal partner for breeding PM-resistant grapevines that are durably resistant and require fewer fungicidal applications. This can be facilitated by functionally characterizing the mechanisms of PM resistance in wild grapes and by introgressing functionally diverse PM resistance-associated genes into *V. vinifera* (Michelmore *et al*., 2013). In wild grapes, PM resistance is associated with a programmed cell death (PCD)-mediated response in infected epidermal cells. This suggests that PM resistance is based on an intracellular recognition of *E. necator*'s effectors by disease resistance (*R*) proteins that activate effector-triggered immunity (Qiu *et al*., 2015; Dry *et al*., 2019).

Most *R* genes encode nucleotide-binding leucine-rich repeat (NLR) proteins (Dubey and Singh, 2018). NLRs are intracellular receptors that recognize and interact directly with pathogen-derived effectors, detect modifications in host cellular targets, or detect molecular decoys triggered by effectors (Dangl *et al*., 2013). NLR activation leads to the induction of immune responses that can restrict pathogen spread (Jones and Dangl, 2006). These include calcium oscillations, a rapid burst of reactive oxygen species (ROS), extensive transcriptional reprogramming that leads to cell wall modifications, and the synthesis of pathogenesis-related (PR) proteins and antimicrobial compounds (Jones and Dangl, 2006; Dangl *et al*., 2013; Kretschmer *et al*., 2019). Effector-triggered immunity is often associated with a hypersensitive response and PCD of infected plant cells that restrict further pathogen development (Jones and Dangl, 2006). NLR intracellular receptors are typically composed of three domains: a C-terminal LRR domain, a central nucleotide-binding site domain (NBS), and a variable N-terminal domain (Meyers *et al*., 1999; McHale *et al*., 2006). The variable N-terminal domain distinguishes NLR classes. The three main NLR classes are the TIR-NBS-LRRs, CC-NBS-LRRs, and RPW8-NBS-LRRs; these possess N-terminal toll/interleukin-1 receptor-like (TIR), Coiled-coil (CC), and resistance to powdery mildew 8 (RPW8) domains, respectively (Meyers *et al*., 1999; McHale *et al*., 2006; Xiao *et al*., 2001; Michelmore *et al*., 2013). Only two TIR-NBS-LRR genes, *MrRPV1* and *MrRUN1*, have been functionally characterized in grapes (Feechan *et al*., 2013). *MrRPV1* and *MrRUN1* are at the *Run1* locus of *M. rotundifolia* G52 and confer resistance to downy mildew and PM, respectively. The first diploid chromosome-scale genome assembly of a muscadine grape was recently published and represents a valuable resource for characterizing the genetic basis of other PM resistance loci in *M. rotundifolia* (Cochetel *et al*., 2021). A first analysis of the *Run1.2* locus suggested an expansion of TIR-NBS-LRR genes in *M. rotundifolia* Trayshed relative to Cabernet Sauvignon (Cochetel *et al*., 2021).

In this study, we describe the structure and content of the *Run1.2* and *Run2.2* loci of *M. rotundifolia* Trayshed and the mechanisms of defense they provide. We evaluated PM disease development in *Run1.2b*$^{+}$ and *Run2.2*$^{+}$ genotypes and thirteen additional accessions that included the loci *Resistance to E. necator 2* (*Ren2*), *Ren3*, *Ren4D*, *Ren4U*, *Run1*, and *Run2.1*. Haplotypes of Trayshed's *R* loci were differentiated and reconstructed by sequencing two backcrossed *V. vinifera* lines carrying either *Run1.2b* or *Run2.2*. Gene models in both loci were manually curated to identify the genes encoding NLRs. To identify NLR genes associated with PM resistance, NLR

genes' expression in *Run1.2b* and *Run2.2* were profiled with and without PM present. Finally, we evaluated the defense mechanisms associated with each of Trayshed's *R* loci by comparing them to six additional *R* loci using RNA-sequencing (RNA-seq).

Results

Run1.2b and *Run2.2* loci exhibit different intensity and timing of the PM response

PM disease development was evaluated on detached leaves from e6-23 (*Run1.2b*$^+$) and 08391-29 (*Run2.2*$^+$), two *V. vinifera* lines into which *Run1.2b* and *Run2.2* loci were introgressed by crossing with *M. rotundifolia* Trayshed and backcrossing with *V. vinifera* (**Supplementary Table S1**). Disease development was also assessed on leaves from their PM-susceptible siblings, e5-96 (*Run1.2b*$^-$) and 08391-28 (*Run2.2*$^-$), and eleven additional grape accessions, including nine interspecific accessions, and two PM-susceptible *V. vinifera,* Malaga Rosada and F2-35 (**Supplementary Table S1**). The nine interspecific hybrids included six siblings derived from backcrosses with one of the following resistant accessions: *V. romanetii* C166-043 (*Ren4D*$^+$), *V. romanetii* C166-026 (*Ren4U*$^+$), or *M. rotundifolia* G52 (*Run1*$^+$) (Ramming *et al*., 2011; Riaz *et al*., 2011; Feechan *et al*., 2013). The remaining three interspecific accessions were 09390-023 (*Ren2*$^+$), 07712-06 (*Ren3*$^+$), and 09705-45 (*Run2.1*$^+$); these inherited PM resistance from *V. cinerea* B9 (Dalbó e*t al.*, 2001), interspecific Villard blanc (Zyprian e*t al.*, 2016), and *M. rotundifolia* Magnolia (Riaz e*t al.*, 2011), respectively.

At 5 days post-inoculation (dpi), PM growth was assessed using microscopy (**Figure 1a**). Little or no mycelia growth was visible on *Run1.2b*$^+$ leaves and the genotypes carrying *Ren4D*, *Ren4U*, *Run1* loci, though some secondary hyphae development was observable on *Run2.2*$^+$, *Ren2*$^+$, *Ren3*$^+$, and *Run2.1*$^+$ genotypes' leaves (**Figure 1a**). In contrast, widespread hyphal growth and conidiophore development were observed on leaves from two PM-susceptible *V. vinifera* cultivars, F2-35 and Malaga Rosada, and all the sibling lines devoid of PM resistance loci (**Figure 1a**). Necrotic spots were observed beneath appressoria of germinated fungal spores and developing secondary hyphae in all the grape accessions possessing a *R* locus. This suggests that a hypersensitive, PCD response occurred in the epidermal cells of these genotypes after pathogen penetration, but at different speeds and levels of efficacy. PM biomass on leaves was also estimated

by measuring *E. necator* transcripts. Genotypes carrying a PM resistance locus had significantly lower *E. necator* transcripts at 5 dpi than genotypes without a PM resistance locus (**Figure 1b,c**). Significant differences in *E. necator* transcripts were also observed between *Run2.2*$^+$, *Ren2*$^+$, and the other PM-resistant accessions (Kruskal-Wallis test followed by post hoc Dunn's test; P value ≤ 0.05).

PM growth was also assessed at an advanced disease development stage (14 dpi) using visual scoring (**Supplementary Figure S1a**). Infection rate at 5 and 14 dpi was similar for all genotypes except *Ren2*$^+$ and *Ren3*$^+$, which both had extensive mycelium growth on their leaves at 14 dpi (Kruskal-Wallis test followed by post-hoc Dunn's test; P value ≤ 0.05). *E. necator* transcript abundance at 5 dpi was correlated with PM infection scores at 14 dpi ($R^2 = 0.73$; **Supplementary Figure S1b**), supporting that quantifying *E. necator* transcript abundance is an effective way to estimate PM susceptibility.

These results show that *R* loci confer post-penetration resistance to PM in *V. vinifera*. However, PM resistance level varies between the *Run1.2b* and *Run2.2* loci, suggesting that Trayshed's *R* loci differ in the perception of the pathogen and/or in the efficiency of the defense response to the pathogen. This implies differences in terms of intracellular receptors (*i.e.*, NLR composition), NLR gene expression, and/or activated defense-related mechanisms between the *Run1.2b* and *Run2.2* loci.

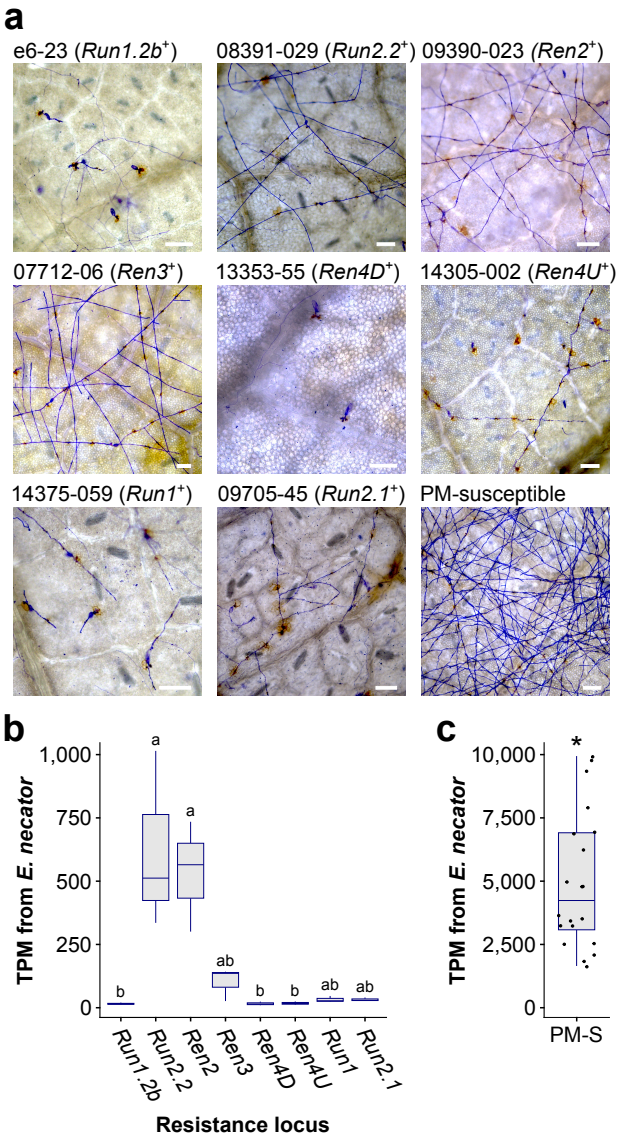

Figure 1: Powdery mildew disease development at 5 days post-inoculation. (**a**) Micrographs of detached leaves stained with Coomassie Brilliant blue to visualize the development of fungal structures on the leaf surface. The 'brown' cells below fungal appressoria are epidermal cells that produced a hypersensitive response (HR) to PM. Scale = 100 µm. Total Transcripts per Million (TPM) derived from *E. necator* transcriptome in PM-resistant (**b**) and PM-susceptible (PM-S) accessions (**c**). Significant differences between PM resistance loci are indicated by different letters (Kruskal-Wallis test followed by post hoc Dunn's test; *P* value ≤ 0.05). Significant differences between genotypes carrying PM resistance loci and PM-susceptible accessions are indicated by an asterisk (Kruskal-Wallis test, *P* value = 1.5×10^{-8}).

Structural variants between Trayshed's *Run1.2* haplotypes affect NLR content

The haplotypes of Trayshed's *R* loci, *Run1.2* and *Run2.2*, were differentiated to determine the effect of NLR composition on PM resistance. The boundaries of *Run1.2* were assigned by aligning the primer sequences of *Run1.2*-associated SSR markers to both haplotypes on *M. rotundifolia* Trayshed chromosome 12 (Cochetel *et al*., 2021). To distinguish *Run1.2a* and *Run1.2b*, we sequenced the *V. vinifera* backcross, e6-23 (*Run1.2b*$^{+}$; **Supplementary Table S1**; **Supplementary Table S2**). Short sequencing reads from the *Run1.2b*$^{+}$ accession covered and aligned perfectly (*i.e*., with no mismatches) to most of *Run1.2* on Haplotype 2 (**Supplementary Figure S2**), and coverage gaps in *Run1.2* on Haplotype 2 were complemented by coverage at *Run1.2* on Haplotype

1. This indicates that haplotype switching occurred during Trayshed assembly and phasing. To correct this, *Run1.2b* was reconstructed using only sequences supported with DNA sequencing reads from e6-23 (*Run1.2b*$^{+}$) and *Run1.2a* was reconstructed using alternative sequences (**Figure 2a**). The reconstructed *Run1.2a* and *Run1.2b* loci were 4.34 Mbp- and 3.38 Mbp-long, respectively. Differences in length between the two haplotypes were associated with several large structural variants (SVs; > 50 bp). For instance, the region of *Run1.2b* from ~12 Mbp to 12.3 Mbp corresponds to a ~800kbp region in the *Run1.2a* haplotype (**Figure 2a**). In this case, length difference was due to several inserted sequences and duplication events in *Run1.2a* compared to *Run1.2b*. We detected 32,704 SNPs and 7,150 INDELs between the two *Run1.2* haplotypes, *Run1.2a* and *Run1.2b*.

We refined the gene models for both *Run1.2* haplotypes to determine the effect of SVs and short polymorphisms at the locus. A total of 78 protein-coding genes, including 22 NLR genes, were manually annotated. *Run1.2a* contained 253 genes and *Run1.2b* contained 189 genes, indicating that SVs affect gene content. There were 37 and 24 NLR genes in *Run1.2a* and *Run1.2b*, respectively, with both composed primarily of CC-NBS-LRR, TIR-NBS-LRR and NBS-LRR genes (**Figure 2a**; **Supplementary Table S3**). SVs between haplotypes affect the protein-coding sequences of 22 NLR genes in *Run1.2a* and 9 NLR genes in *Run1.2b*. Non-synonymous SNPs were identified in 8 NLR genes in each haplotype.

Run2.2 **is mainly composed of TIR-NBS-LRRs**

A similar approach was applied to identify and reconstruct *Run2.2* in the Haplotype 1 of chromosome 18 in *M. rotundifolia* Trayshed using short sequencing reads from the genotype 08391-29 (*Run2.2*$^{+}$) (**Supplementary Tables S1 & S2**; **Supplementary Figure S3**). Reconstructed *Run2.2* was 3.45 Mbp long, slightly longer than its alternative on Haplotype 2 chromosome 18 (3.14 Mbp). We manually refined the models of 102 protein-coding genes in the two haplotypes, including 55 NLR genes. More genes were annotated at *Run2.2* (207) than at its alternative (179). There were 39 NLR-coding genes at *Run2.2* and 29 NLR genes in its alternative. The two haplotypes were mainly composed of TIR-NBS-LRR genes, with 20 genes in *Run2.2* and 21 genes in its alternative (**Supplementary Table S3**). Unlike *Run1.2*, no NLR genes with a CC

or RPW8 N-terminal domain were found at *Run2.2*. Interestingly, the NLR genes occurred in two clusters in each haplotype (**Figure 2b**).

Run2.2 and its alternative on Haplotype 2 chromosome 18 contained 456 SVs between them, with an average length of 2.1 ± 3.6 kbp. There were also 24,128 SNPs and 5,773 INDELs. SVs affected 21 and 16 NLR genes in *Run2.2* and its alternative, respectively, and non-synonymous SNPs were detected in 16 and 18 NLR genes, respectively.

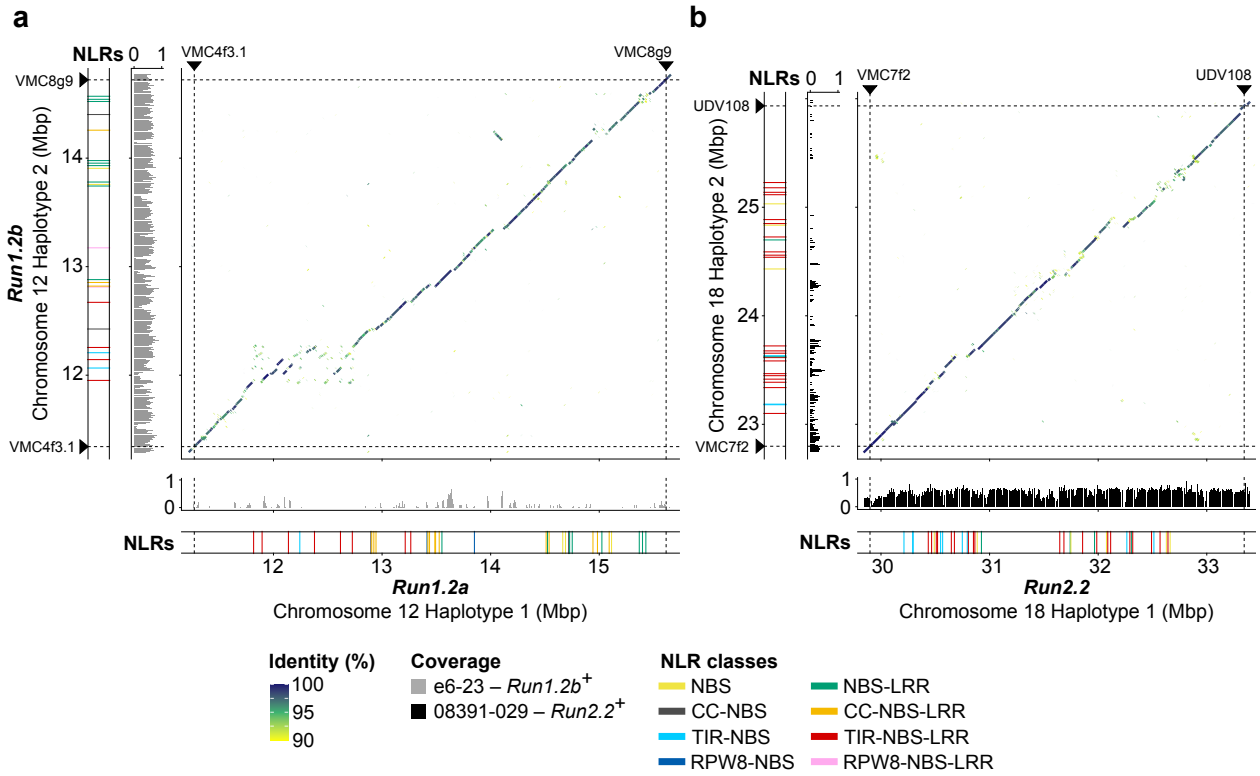

Figure 2: Haplotype comparison and NLR content at *Run1.2* and *Run2.2* in *M. rotundifolia* Trayshed. Whole-sequence alignments of the reconstructed haplotypes of *Run1.2* (**a**) and *Run2.2* (**b**) loci. Normalized median DNA-seq coverage per 10 kbp of e6-23 (*Run1.2b*$^{+}$) and 08391-29 (*Run2.2*$^{+}$) on the diploid genome of *M. rotundifolia* Trayshed was used to identify *Run1.2b* and *Run2.2* on the Haplotype 2 of chromosome 12 and Haplotype 1 of chromosome 18, respectively. Only DNA-seq reads aligning perfectly on the diploid genome of *M. rotundifolia* Trayshed were used for base coverage analysis. Chromosomal position of the *Run1.2*- and *Run2.2*-associated genetic markers is indicated by black triangles and dashed lines.

Run1.2 **and** ***Run2.2*** **loci contain distinct sets of NLRs**

NLRs identified in *Run1.2* and *Run2.2* were compared by constructing a phylogeny using their predicted protein sequences in the four reconstructed haplotypes (*Run1.2a, Run1.2b, Run2.2,* and its alternative on Haplotype 2 chromosome 18; **Figure 3a**). In addition, we compared Trayshed's NLRs with the TIR-NBS-LRRs at *Run1/Rpv1* in *M. rotundifolia* G52 (Barker *et al*., 2005; Feechan *et al*., 2013). *Run1/Rpv1* is the only *R* locus characterized in grapes and is an alternative version of *Run1.2*. Two distinct groups of NLRs were discovered, distinguished by the presence or absence of a TIR domain. A similar clustering pattern was observed when a phylogeny was built using nucleotide-binding domain sequences only (**Supplementary Figure S4**), as previously observed in other plants (Prigozhin and Krasileva, 2021; Seo *et al*., 2016). For TIR-containing proteins, NLRs tended to cluster by *R* locus, with the TIR-NBS-LRRs from *Run1/Rpv1* clustering with TIR-NBS-LRR proteins from *Run1.2*. MrRPV1 from *M. rotundifolia* G52 clustered with two TIR-NBS-LRRs, one from each *Run1.2* haplotype, and MrRUN1 clustered with a TIR-NBS-LRR from *Run1.2a* (**Figure 3a**). However, number of LRR motifs in their LRR domain was different (**Figure 3b**), suggesting that these TIR-NBS-LRRs might be specific to different effectors and/or pathogens.

Run1.2 and *Run2.2* loci are composed of two different sets of NLRs. This may explain why genotypes respond differently to PM. Clustering analyses of TIR-NBS-LRRs in *Run1.2* and *Run1/Rpv1* support an allelic relationship between them, while differences in LRR domains support some allelic diversity in *M. rotundifolia*.

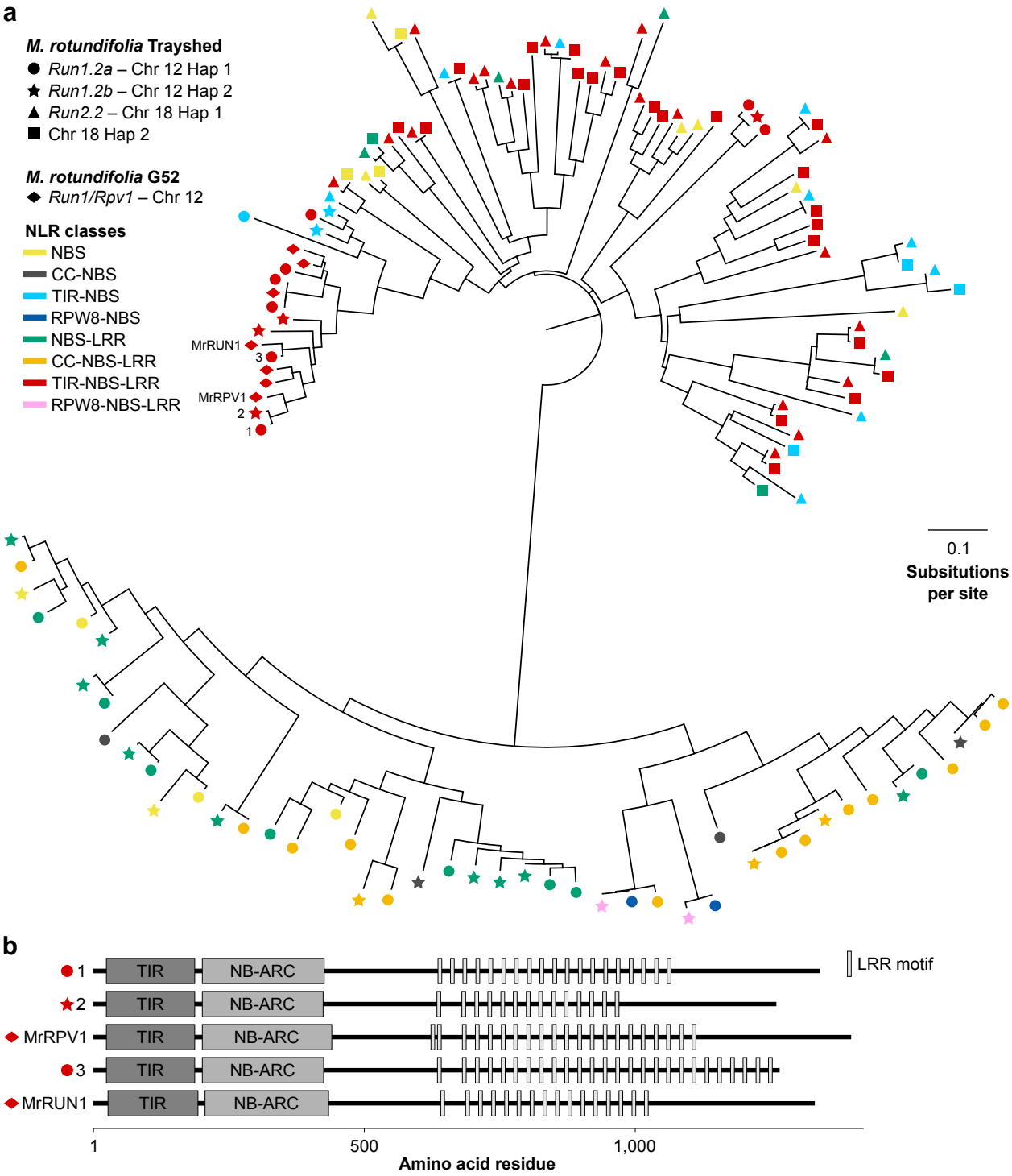

Figure 3: Comparison of the NLRs composing *Run1.2* and *Run2.2* in *M. rotundifolia* Trayshed. (**a**) Neighbor-joining clustering of the predicted NLR protein sequences at *Run1.2*, *Run2.2* and the resistance gene analogs (RGAs) identified at *Run1/Rpv1* (Feechan *et al*., 2013). (**b**) Domain diagram of Trayshed's TIR-NBS-LRRs clustering with G52's MrRUN1 and MrRPV1. Proteins

are reported using same number assigned in panel **a**. LRR motifs were identified using the consensus sequence LxxLxLxx, with L indicating a leucine residue and x indicating any amino acid (Kajava and Kobe, 2002).

NLR genes at *Run1.2b* and *Run2.2* display different levels of transcription

Constitutive NLR gene expression is essential for disease resistance (Michelmore *et al*., 2013). To further characterize Trayshed's loci and identify expressed NLR genes that are potentially responsible for PM resistance, we measured gene expression in *Run1.2b*$^+$ and *Run2.2*$^+$ leaves 1 and 5 days after inoculation with either *E. necator* or a mock solution using RNA-seq (**Figure 4**).

In *Run1.2b*$^+$ leaves, expression of almost all NLR genes from the *Run1.2b* locus (23/24) was detected (**Figure 4a**). Twelve of them were found with an expression level higher than 1 transcript per million (TPM) in at least one condition (TPM > 1), while 11 NLR genes exhibit a lower expression level (TPM ≤ 1). Three genes at the 5'-end of *Run1.2b* encoding two TIR-NBS-LRRs and a TIR-NBS, and a CC-NBS-LRR gene towards the 3'-end were the most highly expressed in all conditions (mean TPM > 4 TPM). In addition, the gene with the most elevated expression was the TIR-NBS-LRR gene which predicted protein clustered with MrRPV1 in the phylogenic tree (**Figure 3**). PM inoculation was found to impact on the gene expression of only one RPW8-NBS-LRR gene at 5 dpi.

In *Run2.2*$^+$ genotype, we identified 12 NLR genes with a transcript abundance superior to 1 TPM, 14 lowly expressed (TPM ≤ 1) and 3 with no expression (**Figure 4b**). A TIR-NBS-LRR gene at the 5'-end of *Run2.2* was the most highly expressed across conditions. Seven other TIR-NBS-LRR genes in the locus had moderate expression levels. Few NLR genes of the *Run2.2* locus were modulated in response to PM. One TIR-NBS-LRR gene was detected as up-regulated in response to PM at 1 dpi, while a TIR-NBS and two TIR-NBS-LRR genes were up-regulated at 5 dpi.

These RNA-seq data show that most of the NLR genes composing Trayshed's loci are expressed independently of the condition, but they exhibit different levels of gene expression in *Run1.2b*$^+$ and *Run2.2*$^+$ genotypes. Expressed NLR genes are candidate genes involved in PM resistance associated with *Run1.2b* and *Run2.2*.

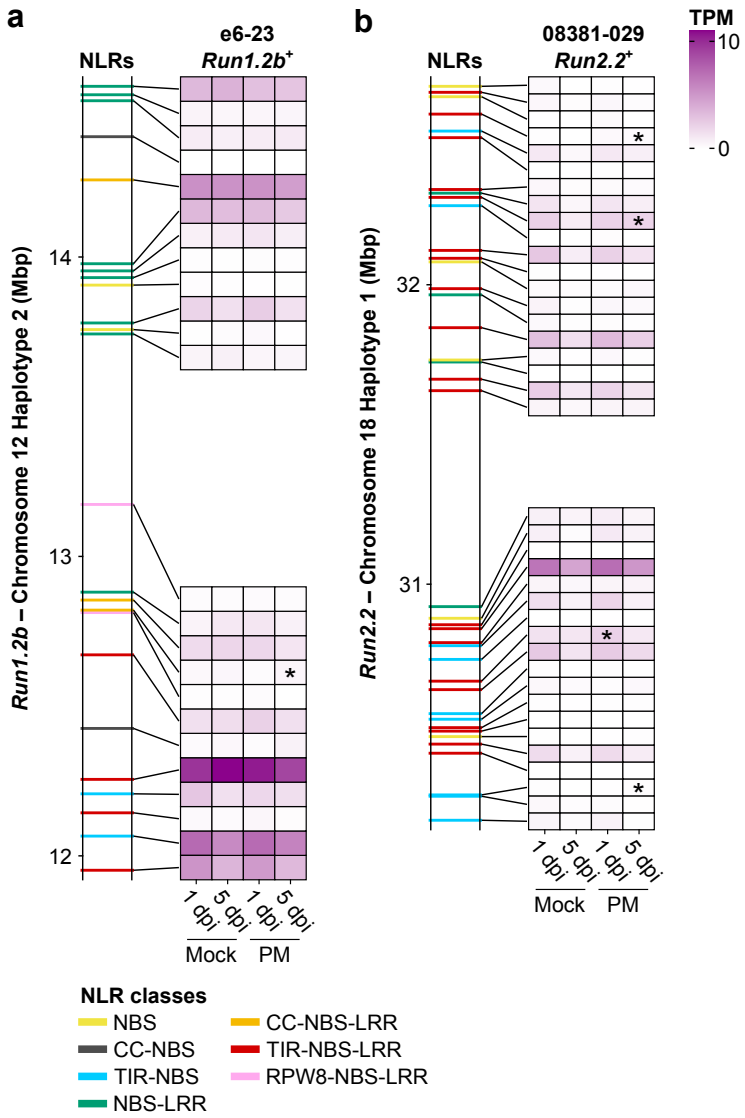

Figure 4: Transcript abundance of NLR genes in *Run1.2b* and *Run2.2*. Gene expression was monitored in *Run1.2b*$^+$ and *Run2.2*$^+$ at 1 and 5 days post inoculation (dpi) with *E. necator* conidia (PM) or a mock solution (Mock). Transcript abundance is shown as the mean of Transcripts per Million (TPM). n = 3. NLR genes differentially expressed in response to PM are indicated by an asterisk (*P* value ≤ 0.05).

Run1.2b and *Run2.2* trigger different defense mechanisms in response to PM and at constitutive level

To determine whether the differences in PM development between *Run1.2b*$^+$ and *Run2.2*$^+$ were due to differences in the pathways induced, we measured the expression of defense-related genes in response to PM in *Run1.2b*$^+$, *Run2.2*$^+$, *Run1.2b*$^-$, *Run2.2*$^-$, and five other PM-susceptible genotypes at 1 and 5 dpi. Six additional PM-resistant genotypes were included to evaluate the functional overlap between Trayshed's *Run1.2b* and *Run2.2* and other sources of resistance that

provide variable level of protection to PM (**Figure 1b**). Because these genotypes are diverse, we constructed comparable reference transcriptomes for each by incorporating variant information and *de novo* assembled transcripts that are not found in PN40024. We also refined the functional annotation of defense genes in the reference transcriptome. We identified 2,694 grape genes involved in the following defense responses: pathogen recognition by receptor-like kinases (RLKs) and intracellular receptors (NLRs), ROS production and scavenging, nitric oxide (NO) production, calcium, MAPK, salicylic acid (SA), jasmonic acid (JA), ethylene (ET), and abscisic acid (ABA) signaling, pathogenesis-related (PR) protein and phytoalexin biosynthesis, and cell wall reinforcement (**Supplementary Table S4**).

Comparison between PM- and mock-inoculated leaf transcriptomes showed a similar number of defense-related genes up-regulated in *Run1.2b*$^+$ and *Run2.2*$^+$ in response to the pathogen at 1 dpi, with 165 and 135 genes, respectively (**Supplementary Figure S5**). Number of up-regulated genes decreased at 5 dpi in *Run1.2b*$^+$ (69) related to 1 dpi, whereas a higher number of up-regulated genes (449) was identified in *Run2.2*$^+$.

To identify the transcriptional modulation associated with PM resistance, genes up-regulated in response to PM in e6-23 (*Run1.2b*$^+$) and 08391-29 (*Run2.2*$^+$) were then compared with the ones detected in their PM-susceptible siblings, e5-96 (*Run1.2b*$^-$) and 08391-28 (*Run2.2*$^-$), and the five additional PM-susceptible genotypes (**Figure 5a**). This comparison impacted substantially the number of up-regulated genes in the genotypes possessing Trayshed's *R* loci, especially *Run2.2*$^+$, in which only 13 of the 449 up-regulated genes at 5 dpi were associated with resistance to PM. The number of up-regulated resistance- and defense-related genes were similar in *Run1.2b*$^+$ and *Run2.2*$^+$ at both time points.

Among the 68 genes up-regulated in *Run1.2b*$^+$ at 1 dpi, two encode Respiratory Burst Oxidase Homologs, which participate in ROS production (Suzuki *et al*., 2011), three are associated with calcium signaling, three encode PR proteins, 13 are involved in phytoalexin biosynthesis, and one is a homolog of SENESCENCE-ASSOCIATED GENE 101 (SAG101). In *Arabidopsis thaliana*, SAG101 contributes to the SA-mediated response and is required for PCD (Feys *et al*., 2005). Interestingly, this SAG101-like gene was up-regulated in response to PM at 5 dpi in *Run2.2*$^+$ and in five PM-susceptible accessions. Of the 41 genes identified as up-regulated in *Run2.2*$^+$ at 1 dpi and associated with PM resistance, 5 genes encode PR proteins, 5 are involved in terpenoid

biosynthesis, 4 in ABA-signaling, and 3 in JA-mediated signaling pathways. Almost half (47.3%) of the up-regulated genes associated with PM resistance in *Run1.2b*$^{+}$ and *Run2.2*$^{+}$ were also up-regulated by another *R* locus (**Figure 5a,b**), indicating some functional overlap among them.

Transcriptomes of mock-inoculated leaves from *Run1.2b*$^{+}$, *Run2.2*$^{+}$, and six additional PM-resistant genotypes were compared to seven PM-susceptible genotypes to check for constitutive PM resistance. *Run1.2b*$^{+}$ had one of the greatest number of highly constitutively expressed defense genes (121 genes at 1 dpi, 133 genes at 5 dpi; **Figure 5c,d**). Among these genes, we found several genes encoding RLKs and NLRs and genes involved in ROS production and scavenging, SA-mediated signaling, phenylpropanoid biosynthesis, and cell wall reinforcement. Many of these, including the SAG101-like gene, were more highly expressed specifically in *Run1.2b*$^{+}$ versus other PM-resistant accessions. In *Run2.2*$^{+}$, 6 genes involved in flavonoid biosynthesis were associated with PM resistance at 1 dpi. At 1 dpi and 5 dpi, 5 genes coding for laccases were most highly expressed in *Run2.2*$^{+}$. Laccases are enzymes involved in lignin polymerization, an important component of plant cell wall structural strength (Zhao *et al*., 2013). Constitutively elevated laccase gene expression might thicken the secondary cell wall in leaves, thus providing a physical barrier to pathogens (Miedes *et al*., 2014) in *Run2.2*$^{+}$.

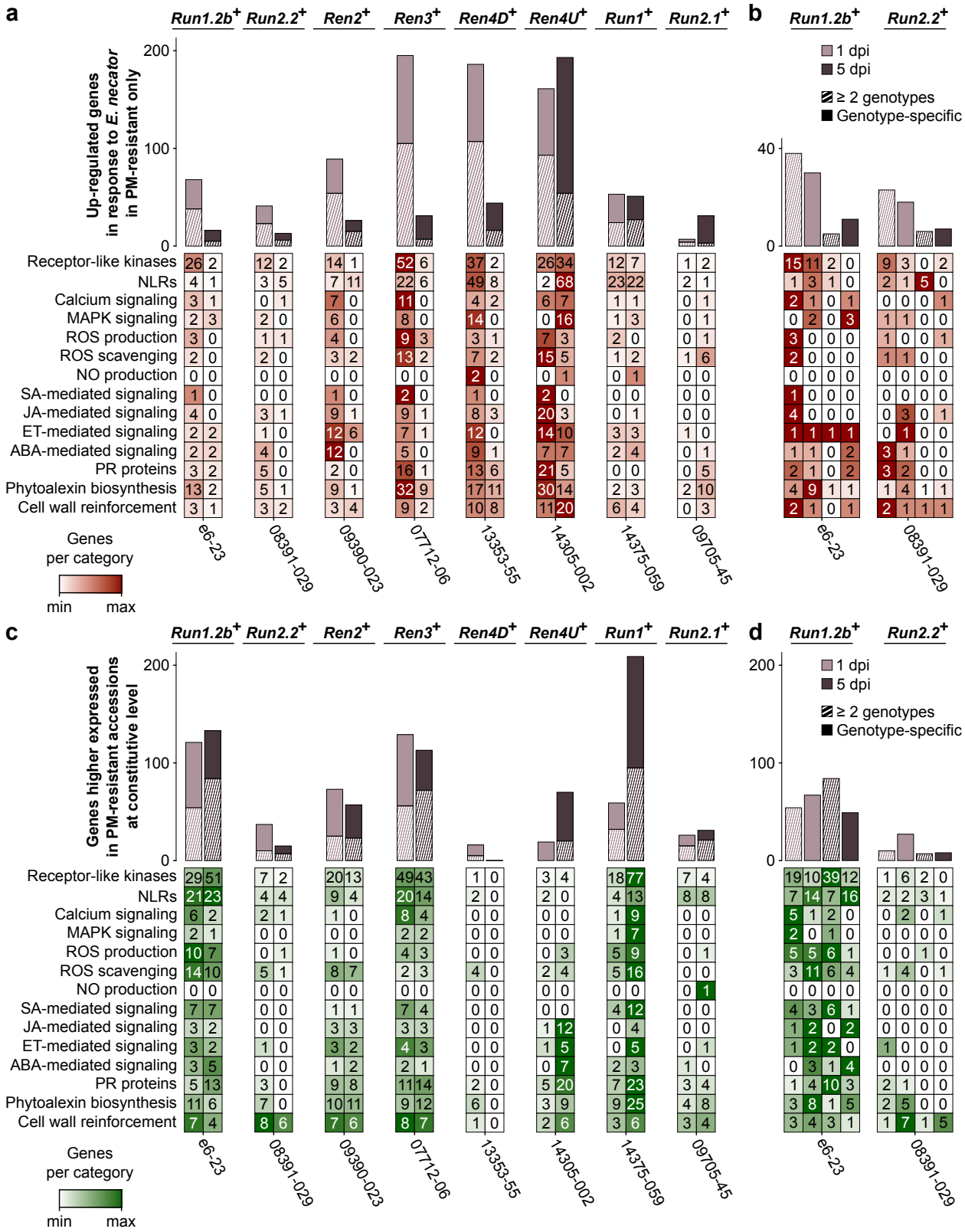

Figure 5: PM resistance-associated gene expression in defense signaling pathways. (**a**) Defense-related genes uniquely up-regulated by *E. necator* in PM-resistant accessions and (**c**) genes with

higher constitutive expression in PM-resistant genotypes than seven PM-susceptible genotypes. For each comparison, gene overlap between e6-23 (*Run1.2b*$^{+}$) and 08391-29 (*Run2.2*$^{+}$) and the other PM-resistant accessions is detailed in panels (**b**) and (**d**).

Discussion

Trayshed's *Run1.2b* and *Run2.2 R* loci provide resistance to PM in *V. vinifera* via different defense mechanisms

Introgression of Trayshed's *Run1.2b* and *Run2.2* loci into two *V. vinifera* lines confers post-penetration resistance to PM, but at different speeds and intensities (**Figure 1**). Similar disease phenotypes have been described in previous studies (Qiu *et al*., 2015; Dry *et al*., 2019). This suggests that the intracellular perception *of E. necator* and/or the efficiency of the defense mechanisms activated by Trayshed's NLRs consequentially differ. To test the latter hypothesis, we profiled the expression of selected defense-related genes in PM- and mock-inoculated leaves from *Run1.2b*$^{+}$*, Run2.2*$^{+}$, six other *R* locus-containing accessions, and seven PM-susceptible accessions with diverse genetic backgrounds. The genes with an expression associated with PM resistance, *i.e*. the genes up-regulated by PM only in PM-resistant accessions and genes constitutively higher expressed in PM-resistant *vs*. PM-susceptible genotypes, differed in *Run1.2b*$^{+}$ and *Run2.2*$^{+}$. In particular, the difference of timing of the up-regulation of a SAG101-like gene suggests that SA-associated response and thus PCD might be delayed in the *Run2.2*$^{+}$ genotype. This hypothesis could be tested by profiling defense-related gene expression in additional accessions carrying Trayshed's *R* loci and by measuring SA content in both mock- and PM-inoculated leaves. Differences in defense mechanisms associated with *Run1.2b* and *Run2.2* loci also suggest that Trayshed's PM resistance could be due to the synergic effect of its *R* loci. Previous studies have showed that stacking *R* loci could enhance PM resistance (Feechan *et al*., 2015; Agurto *et al*., 2017). It would be interesting to evaluate the effect of introgressing both Trayshed's *R* loci. Furthermore, comparison of the *R* loci showed some functional overlap between the eight PM-resistant accessions, but it also highlighted defense mechanisms specific to each *R* locus. The generated data could serve to estimate the best combination of functionally diverse PM

resistance-associated loci to stack and introgress into wine grapes for durable resistance to PM (Michelmore *et al*., 2013).

Haplotype resolution of *Run1.2* and *Run2.2* loci identifies distinct NLR composition

By combining a diploid assembly of Trayshed's genome and DNA sequencing data generated from two backcrossed *V. vinifera* genotypes, we distinguished and reconstructed both haplotypes of *Run1.2* and *Run2.2* loci. To our knowledge, this is the first report of complete, haplotype-resolved *R* loci for grape. The *Run1*/*Rpv1* locus was sequenced prior, but its assembly was fragmented and haploid (Feechan *et al*., 2013). Deep sequencing *Run1.2a*$^{+}$ genotypes and accessions possessing the alternative *Run2.2* haplotype would help to validate the NLR composition of these two haplotypes. Trayshed was previously defined as homozygous at *Run2.2 locus* based on amplicon size (Riaz *et al*., 2011). However, *in silico* PCR on Trayshed's genome showed two amplicon sizes for the UDV108 marker: 225 bp on chromosome 18 Haplotype 1 and 323 bp on chromosome 18 Haplotype 2. Sequencing additional *Run2.2*$^{+}$ backcrossed individuals would help determine whether the region on chromosome 18 Haplotype 2 is associated with PM resistance.

Whole-sequence comparison and manual gene model refinement of the two reconstructed haplotypes of each Trayshed's *R* locus revealed numerous SVs and short polymorphisms affecting the sequences of multiple NLR genes for both *Run1.2b* and *Run2.2* loci. A total of 77 NLR genes required manual annotation, representing ~60% of the NLR genes identified among the four haplotypes. This highlights the necessity of generating phased haplotypes and meticulously dissecting complex genomic regions if trait-associated candidate genes are sought (Massonnet *et al*., 2020).

The NLRs in Trayshed's *Run1.2* and *Run2.2* loci were different. All three classes of NLRs, CC-NBS-LRRs, RPW8-NBS-LRRs and TIR-NBS-LRRs were found in *Run1.2* haplotypes, but no CC or RPW8 domains were identified among NLRs at *Run2.2*. The only characterized NLR gene associated with grape PM resistance, MrRUN1, is a TIR-NBS-LRR (Feechan *et al*., 2013). Functional characterization of the NLR genes composing Trayshed's *R* loci would help identify the NLR(s) responsible for PM resistance and to determine whether the NLR class is a decisive factor for grape PM resistance.

Finally, the approach used in this study could be applied to other *R* loci, giving new opportunities for functional genomics. However, fine mapping or generation of sequencing data (DNA-seq and RNA-seq) from recombinants would be necessary to narrow down candidate NLR genes associated with PM resistance.

Materials and methods

Plant material

Fifteen grape accessions were used in this study, including eight carrying a powdery mildew (PM) resistance (*R*) locus. The genotypes comprised ten sister lines derived from crosses between a susceptible parent and a parent with an *R* locus. Information about the lineage of each genotype is provided in **Supplementary Table S1**.

For each accession, three plants were mock-inoculated and three plants were PM-inoculated in separate Conviron PGR15 growth chambers (UC Davis Controlled Environment Facility) maintained at identical environmental conditions (60% humidity, 23°C during the day for 16 hours, 15°C during the night). *E. necator* isolate C-strain conidia were amplified on *in vitro* cultures of detached *V. vinifera* Carignan leaves, suspended in 0.001 % (v/v) Tween solution, and adjusted to 5×10^5 conidia mL^{-1}. Conidia or a 0.001% Tween solution were applied to leaves using a Preval Sprayer unit (Chicago Aerosol, Coal City, Illinois). Two leaves from each plant were collected 1 and 5 dpi, at the same time of day, and immediately frozen in liquid nitrogen. Leaves from an individual plant were pooled together and constitute a biological replicate. Three biological replications were obtained for each treatment.

Assessment of PM susceptibility

PM susceptibility was evaluated with a detached leaf assay as described in Pap *et al*. (2016). Leaves of each accession were surface-sterilized in 0.3% sodium hypochlorite solution and inoculated with two-week-old *E. necator* C-strain conidia using a custom-made settling tower (Reifschneider and Boiteux, 1988). Disease severity was assessed by visually scoring infection rate under a microscope Leica EZ4 D at 14 dpi (**Supplementary Figure S1a**). Two people independently rated PM growth using a 0–4 scale as described in Pap *et al*. (2016): 0 = no hypha;

1 = few germinated conidia per leaf with only primary hyphae; 2 = several conidia with primary and, in some cases, secondary hyphae; 3 = mycelium is visible on the entire leaf surface with limited conidiophores; 4 = mycelia coverage is extensive with extensive conidiation, clearly visible with the naked eye. Visual scores per genotype (**Supplementary Figure S1a**) were compared using a Kruskal-Wallis test followed by a post hoc Dunn's test (P-value ≤ 0.05). Detached leaves were stained with Coomassie Brilliant Blue R-250 at 5 dpi using the procedure described in Riaz *et al.* (2013).

DNA and RNA extraction, library preparation, and sequencing

Genomic DNA were isolated from e6-23 (*Run1.2b*$^{+}$) and 08391-029 (*Run2.2*$^{+}$) mock-inoculated leaves as described in Chin *et al*. (2016). DNA purity was evaluated using a Nanodrop 2000 spectrophotometer (Thermo Scientific, IL, USA). DNA quantity was estimated with Qubit 2.0 Fluorometer (Thermo Scientific, IL, USA). One microgram of high-quality DNA was fragmented by sonication using a E220 ultrasonicator (Covaris, Woburn, MA, US). Fragmented DNA was used as a template for library preparation using the Kapa LTP library prep kit (Kapa Biosystems, Wilmington, MA, US). Size selection after ligating adapters was done with the eGel system (Invitrogen, Carlsbad, CA, USA). Final libraries were evaluated for quantity and quality using a Bioanalyzer 2100 (Agilent Technologies, CA) and sequenced on the Illumina HiSeqX Ten system in paired-end 150-bp reads (IDseq Inc) (**Supplementary Table S2**).

Total RNA was extracted using a Cetyltrimethyl Ammonium Bromide (CTAB)-based extraction protocol as described in Blanco-Ulate *et al*. (2013). RNA concentration and purity were evaluated using a Qubit fluorometer (Thermo Scientific) and a NanoDrop 2000c Spectrophotometer (Thermo Scientific), respectively. Sequencing libraries were prepared using the Illumina TruSeq RNA sample preparation kit v.2 (Illumina, CA, USA). Quality control of size and purity of the final libraries was assessed using the High Sensitivity DNA kit on a Bioanalyzer 2100 (Agilent Technologies, CA). cDNA libraries were sequenced using Illumina HiSeq2500 and HiSeq4000 sequencers (DNA Technologies Core, University of California, Davis, CA, USA) as 50-bp single-end reads (**Supplementary Table S5**).

Locus reconstruction

Run1.2 and *Run2.2* were identified by aligning VMC4f3.1 and VMC8g9 marker primers to *Run1.2* and VMC7f2 and UDV108 marker primers to *Run2.2* locus (Riaz *et al*., 2011). Whole-genome DNA sequencing reads from e6-23 (*Run1.2b*$^{+}$) and 08391-29 (*Run2.2*$^{+}$) were then used to identify *Run1.2b* and *Run2.2* sequences. Low-quality DNA sequencing reads were removed and adapter sequences were trimmed using Trimmomatic v.0.36 (Bolger *et al*., 2014) with the following settings: LEADING:3 TRAILING:3 SLIDINGWINDOW:10:20 MINLEN:36 CROP:150. High-quality paired-end reads were aligned onto the diploid *M. rotundifolia* Trayshed genome (Cochetel *et al*., 2021) using BWA v.01.17 (Li and Durbin, 2009) and default parameters. Reads aligning on the reference genome with no edit distance (0 mismatch), were selected using bamtools filter v.2.5.1 (Barnett *et al*., 2011) and the tag "NM:0". These reads were used as input for evaluating base coverage with genomecov (BEDTools v2.29.1; Quinlan, 2014). Coverage from bases located in repetitive elements were removed using BEDTools intersect v2.29.1 (Quinlan, 2014). Median coverage per 10 kbp was calculated using an in-house R script and normalized by dividing by the sequencing coverage. Sequences were removed from the locus and labeled "unplaced" if DNA sequencing reads did not cover a primary contig nor its alternative haplotigs. Each haplotype was fragmented into 1 kbp sequences using seqkit sliding v.0.16.1 (Shen *et al*., 2016) and aligned to itself using Minimap2 v.2.12-r847-dirty (Li, 2018) to find sequence overlaps between contigs and remove them from the locus. DNA sequencing coverage along the four haplotypes was manually inspected by visualizing alignments using Integrative Genomics Viewer (IGV) v.2.4.14 (Robinson *et al*., 2011). Loci were reconstructed using the script HaploMake.py from the tool suite HaploSync v1.0 (https://github.com/andreaminio/HaploSync).

Haplotype sequence comparison

Pairwise alignments were performed using NUCmer from MUMmer v.4.0.0 (Marçais *et al*., 2018) with the option --mum. Alignments with at least 90% identity are shown in **Figure 2**. Structural variants (SVs; >50 bp) and short INDELs (<50 bp) were called using show-diff and show-snps, respectively from MUMmer v.4.0.0 (Marçais *et al*., 2018).

Annotation of NLR genes

The genome was scanned with NLR-annotator using default parameters (Steuernagel *et al*., 2020). Gene models within the *R* loci were manually refined by visualizing alignments of RNA-seq reads from Trayshed (Cochetel *et al*., 2021), e6-23 (*Run1.2b*$^{+}$), and 08391-29 (*Run2.2*$^{+}$) leaves using

Integrative Genomics Viewer (IGV) v.2.4.14 (Robinson *et al*., 2011). RNA-seq reads were aligned onto the diploid genome of *M. rotundifolia* Trayshed using HISAT2 v.2.1.0 (Kim *et al*., 2015) and the following settings: --end-to-end --sensitive -k 50.

Predicted proteins were scanned with hmmsearch from HMMER v.3.3.1 (http://hmmer.org/) and the Pfam-A Hidden Markov Models (HMM) database (El-Gebali *et al*., 2019; downloaded on January 29th, 2021). Protein domains corresponding to the following Pfam domains: NB-ARC (PF00931.23), LRR (PF00560.34, PF07725.13, PF12799.8, PF13306.7, PF13516.7, PF13855.7), TIR (PF01582.21, PF13676.7), RPW8 (PF05659.12), with an independent E-value less than 1.0, and an alignment covering at least 50% of the HMM were selected (**Supplementary Table S3**). Coiled-coil (CC) domain-containing proteins were identified by COILS (Lupas *et al*., 1991). Proteins were divided into eight protein classes according to their domain composition: NBS, CC-NBS, NBS-LRR, TIR-NBS, RPW8-NBS, CC-NBS-LRR, TIR-NBS-LRR, and RPW8-NBS-LRR.

Phylogenetic analysis

Predicted NLR protein sequences from Trayshed's *Run1.2* and *Run2.2* and G52's *Run1/Rpv1* (Feechan *et al*., 2013) were aligned using MUSCLE (Edgar, 2004) in MEGAX (Kumar *et al*., 2018). Resistance gene analogs (RGAs) from *Run1/Rpv1* (Feechan *et al*., 2013) were retrieved on GenBank using the following accession numbers: RGA1, AGC24025; RGA2, AGC24026; RGA4, AGC24027; MrRPV1 (RGA8), AGC24028; RGA9, AGC24029; MrRUN1 (RGA10), AGC24030; RGA11, AGC24031. Phylogenetic analysis of the proteins was performed with MEGAX (Kumar *et al*., 2018) using the Neighbor-Joining method (Saitou and Nei, 1987) and 1,000 replicates. Evolutionary distances were computed using the Poisson correction method (Zuckerkandl and Pauling, 1965) and are expressed as the number of amino acids or base substitutions per site. Positions with less than 5% site coverage were eliminated.

Reference transcriptome reconstruction

For each accession, we constructed a reference transcriptome composed of a diploid synthetic transcriptome and *de novo* assembled transcripts. The diploid synthetic transcriptome was reconstructed using variant information. First, adapter sequences were removed and RNA-seq reads were filtered based on their quality using Trimmomatic v.0.36 (Bolger *et al*., 2014) and these settings: LEADING:3 TRAILING:3 SLIDINGWINDOW:10:20 MINLEN:20. Quality-trimmed

reads of the 12 samples from each accession were concatenated into a single file and mapped onto a combined reference genome composed of *V. vinifera* PN40024 V1 (Jaillon *et al*., 2007) and *E. necator* C-strain genome (Jones *et al*., 2014) following the STAR 2-pass mapping protocol (v.2.5.3a; Dobin *et al*., 2013; Engstrom *et al*., 2013). PCR and optical duplicates were removed with Picard tools (v.2.0.1 http://broadinstitute.github.io/picard/), and reads were split into exon segments using SplitNCigarReads from GATK v.3.5-0-g36282e4 (McKenna *et al*., 2010). GATK HaplotypeCaller was used to call sequence variants with the following parameters: -ploidy 2 -stand_call_conf 20.0 -stand_emit_conf 20.0 -dontUseSoftClippedBases. Variants were filtered using GATK VariantFiltration with these settings: -window 35 -cluster 3 -filterName FS -filter "FS > 30.0" -filterName QD -filter "QD < 2.0". Variants passing all filters were selected using GATK SelectVariants with "--excludeFiltered" parameter. On average, 265,721 ± 38,043 variants were detected per genotype (**Supplementary Table S6**). Variants in grape protein-coding regions were selected using bedtools intersect v.2.19.1 (Quinlan, 2014). Two separate genomes were reconstructed for each genotype using the vcf-consensus tool from vcftools (Danecek *et al*., 2011). The first genome was reconstructed by incorporating both homozygous and heterozygous alternative 2 (ALT2) variants in PN40024 V1, while the second genome was reconstructed using both homozygous and heterozygous alternative 1 (ALT1) variants. A new annotation file (gff3) was created for each genome from its corresponding variant information. CDS were extracted using gffread from Cufflinks v.2.2.1 (Trapnell *et al*., 2010).

For each genotype, quality-trimmed reads were mapped onto the combined reference transcriptome consisting of its diploid synthetic grape transcriptome and *E. necator* C-strain CDS (Jones *et al*., 2014) using Bowtie2 v.2.3.4.1 (Langmead and Salzberg, 2012) and these parameters: --end-to-end --sensitive --un. For each genotype, *de novo* assembly was performed using unmapped reads from the 12 RNA-seq libraries and TRINITY v.2.4.0 (Grabherr *et al*., 2011). A total of 550,369 sequences were reconstructed, corresponding to 36,691 ± 2,694 sequences per accession (**Supplementary Table S7**). To reduce sequence redundancy, reconstructed transcripts from all 15 genotypes were clustered using CD-HIT-EST v.4.6.8 (Li and Godzik, 2006) and an identity threshold of 90%. The longest representative sequence of each of the 102,391 CD-HIT clusters was used as input for TransDecoder v.3.0.1. CDS redundancy was again reduced by clustering using CD-HIT-EST v.4.6.8 (Li and Godzik, 2006), with coverage and identity thresholds of 100%. In total, 2,137 CDS were retained (**Supplementary Data S1**). Taxonomic

analysis of the predicted proteins was performed using Megan v.6.12.5 (Huson *et al*., 2016) with default parameters after aligning predicted peptides against the RefSeq protein database (ftp://ftp.ncbi.nlm.nih.gov/refseq, retrieved January 17th, 2017). Peptides assigned to proteobacteria, opisthokonts, and viruses were considered microbial contaminants (**Supplementary Table S8**).

Gene expression analysis

Transcript abundance was evaluated using Salmon v.1.5.1 (Patro *et al*., 2017) and these parameters: --gcBias --seqBias --validateMappings. For assessing the NLR gene expression in e6-23 (*Run1.2b*$^{+}$) and 08391-29 (*Run2.2*$^{+}$), transcriptomes of *M. rotundifolia* Trayshed and *E. necator* C-strain (Jones *et al*., 2014) were combined, and their genomes were used as decoy. To study the expression of defense-related genes, the diploid synthetic transcriptomes of each grape accession was combined with the *de novo* assembled transcripts and the *E. necator* C-strain transcriptome. The PN40024 V1 and *E. necator* C-strain genomes were used as decoys. Transcriptome index files were built with a k-mer size of 13. Quantification files were imported using the R package tximport v.1.20.0 (Soneson *et al*., 2015). Read counts of the two haplotypes of each locus of the diploid synthetic transcriptome were combined. Read-count normalization of the grape transcripts and statistical testing of differential expression were performed using DESeq2 v.1.16.1 (Love *et al*., 2014). One sample (14305-001_H_5dpi_1) was removed from the RNA-seq analysis because of its low mapping rate (**Supplementary Table S5**).

Functional annotation of the defense-related genes

Grape and *Arabidopsis thaliana* predicted proteins were scanned with hmmsearch from HMMER v.3.3.1 (http://hmmer.org/) and the Pfam-A Hidden Markov Models (HMM) database (El-Gebali *et al*., 2019; downloaded on January 29th, 2021). Protein domains with an independent E-value less than 1.0 and an alignment covering at least 50% of the HMM were selected. Grape proteins were aligned onto *A. thaliana* proteins (Araport11_genes.201606.pep.fasta; https://www.arabidopsis.org/download/index.jsp) using BLASTP v.2.6.0. Alignments with an identity greater than 30% and a reciprocal target:query coverage between 75% and 125% were kept. For each grape protein, the best hit in the *A. thaliana* proteome was determined using the highest product of identity, query coverage, and reference coverage. Genes involved in each

defense-related category was manually curated based on literature. The functional annotation of defense-related genes used in this study can be found in **Supplementary Table S5**.

Data availability

Sequencing data are accessible through NCBI under the BioProject ID PRJNA780568. New genome assembly of *M. rotundifolia* Trayshed and annotation files are available at Zenodo under the DOI 10.5281/zenodo.5703495 and at www.grapegenomics.com.

Acknowledgements

This work was partially funded by the American Vineyard Foundation grant #2017–1657 and the US Department of Agriculture (USDA)-National Institute of Food and Agriculture (NIFA) Specialty Crop Research Initiative award #2017-51181-26829, and partially supported by funds to D.C. from Louis P. Martini Endowment in Viticulture.

Conflict of interests

The authors declare no conflict of interest.

Contributions

D.C, M.A.W, S.R, and M.M. designed the project. S.R and D.P performed sample inoculation, collection, microscopy and visual scoring. R.F.-B. extracted DNA and RNA and prepared sequencing libraries. M.M., N.C., A.M performed data analyses. M.M, A.M.V, and D.C wrote the manuscript.

Supplementary information accompanies the manuscript on the Horticulture Research website http://www.nature.com/hortres

References

Agurto, M. *et al*. *RUN1* and *REN1* pyramiding in grapevine (*Vitis vinifera* cv. Crimson Seedless) displays an improved defense response leading to enhanced resistance to powdery mildew (*Erysiphe necator*). *Front Plant Sci.* **8**, 758 (2017).

Barker, C. L. *et al*. Genetic and physical mapping of the grapevine powdery mildew resistance gene, *Run1*, using a bacterial artificial chromosome library. *Theor. Appl. Genet.* **111**, 370–377 (2005).

Barnett, D. W., Garrison, E. K., Quinlan, A. R., Strömberg, M. P. & Marth, G. T. BamTools: a C++ API and toolkit for analyzing and managing BAM files. *Bioinformatics* **27(12)**, 1691–1692 (2011).

Blanco-Ulate, B., Vincenti, E., Powell, A. L. T. & Cantu, D. Tomato transcriptome and mutant analyses suggest a role for plant stress hormones in the interaction between fruit and *Botrytis cinerea*. *Front. Plant Sci.* **4**, 142 (2013).

Bolger, A. M., Lohse, M. & Usadel, B. Trimmomatic: a flexible trimmer for Illumina sequence data. *Bioinformatics* **30**, 2114–2120 (2014).

Chin, C.-S. *et al*. Phased diploid genome assembly with single-molecule realtime sequencing. *Nat. Methods* **13**, 1050–1054 (2016).

Cochetel, N. *et al*. Diploid chromosome-scale assembly of the *Muscadinia rotundifolia* genome supports chromosome fusion and disease resistance gene expansion during *Vitis* and *Muscadinia divergence*. *G3 (Bethesda, Md.)* **11(4)**, jkab033 (2021).

Dalbó, M. A., Ye, G. N., Weeden, N. F., Wilcox, W. F. & Reisch, B. I. Marker-assisted selection for powdery mildew resistance in grapes. *J Amer Soc Hort Sci* **126(1)**, 83–89 (2001).

Danecek, P. *et al*. The variant call format and VCFtools. *Bioinformatics* **27(15)**, 2156–2158 (2011).

Dangl, J. L., Horvath, D. M. & Staskawicz, B. J. Pivoting the plant immune system from dissection to deployment. *Science* **341(6147)**, 746–751 (2013).

Dobin, A. *et al*. STAR: ultrafast universal RNA-seq aligner. *Bioinformatics* **29**, 15–21 (2013).

Dry, I., Riaz, S., Fuchs, M., Sosnowski M. & Thomas, M. Scion Breeding for Resistance to Biotic Stresses. In The Grape Genome (eds Cantu, D. & Walker, M. A) Ch. 15 (Spinger, 2019).

Dubey, N. & Singh, K. Role of NBS-LRR Proteins in Plant Defense. In Molecular Aspects of Plant-Pathogen Interaction (eds Singh A. & Singh I.) (Springer, 2018).

Edgar, R. C. MUSCLE: multiple sequence alignment with high accuracy and high throughput. *Nucleic Acids Res.* **32**, 1792–1797 (2004).

Finn, R. D. *et al*. The Pfam protein families database. *Nucleic Acids Res.* **36**(Database issue), D281–D288 (2008).

Engstrom, P. G. *et al*. Systematic evaluation of spliced alignment programs for RNA-seq data. *Nat Methods* **10**, 1185–1191 (2013).

Feechan, A. *et al*. Genetic dissection of a TIR-NB-LRR locus from the wild North American grapevine species *Muscadinia rotundifolia* identifies paralogous genes conferring resistance to major fungal and oomycete pathogens in cultivated grapevine. *Plant J.* **76**, 661–674 (2013).

Feechan, A. *et al*. Strategies for *RUN1* deployment using *RUN2* and *REN2* to manage grapevine powdery mildew informed by studies of race specificity. *Phytopathology* **105(8)**, 1104–1113 (2015).

Feys, B. J. *et al*. Arabidopsis SENESCENCE-ASSOCIATED GENE101 stabilizes and signals within an ENHANCED DISEASE SUSCEPTIBILITY1 complex in plant innate immunity. *Plant Cell* **17(9)**, 2601–2613 (2005).

Gadoury, D. M. *et al*. Grapevine powdery mildew (*Erysiphe necator*): a fascinating system for the study of the biology, ecology and epidemiology of an obligate biotroph. *Mol Plant Pathol.* **13**,1–16 (2012).

Grabherr, M. G. *et al*. Trinity: reconstructing a full-length transcriptome without a genome from RNA-Seq data. *Nature Biotechnol.* **29(7)**, 644–652 (2011).

Huson, D. H. *et al*. MEGAN community edition - Interactive exploration and analysis of large-scale microbiome sequencing data. *PLoS Computl Biol*. **12(6)**, e1004957 (2016).

Jaillon, O. *et al*. The grapevine genome sequence suggests ancestral hexaploidization in major angiosperm phyla. *Nature* **449**, 463–468 (2007).

Jones, J. & Dangl, J. The plant immune system. *Nature* **444**, 323–329 (2006).

Jones, L. *et al*. Adaptive genomic structural variation in the grape powdery mildew pathogen, *Erysiphe necator*. *BMC Genomics* **15(1)**, 1081 (2014).

Kajava, A. V. & Kobe, B. Assessment of the ability to model proteins with leucine-rich repeats in light of the latest structural information. *Protein Sci* **11**, 1082–1090 (2002).

Karn, A. *et al*. Discovery of the *REN11* locus from *Vitis aestivalis* for stable resistance to grapevine powdery mildew in a family segregating for several unstable and tissue-specific quantitative resistance loci. *Front Plant Sci.* **12**, 733899 (2021).

Kretschmer, M., Damoo, D., Djamei, A. & Kronstad, J. Chloroplasts and plant immunity: Where are the fungal effectors? *Pathogens* **9(1)**, 19 (2019).

Kumar, S., Stecher, G., Li, M., Knyaz, C. & Tamura, K. MEGA X: Molecular Evolutionary Genetics Analysis across computing platforms. *Mol Biol Evol.* **35**, 1547–1549 (2018).

Langmead, B. & Salzberg, S. L. Fast gapped-read alignment with Bowtie 2. *Nature Methods* **9(4)**, 357–359 (2012).

Li, H. & Durbin, R. Fast and accurate short read alignment with Burrows−Wheeler transform. *Bioinformatics* **25(14)**, 1754–1760 (2009).

Li, H. Minimap2: pairwise alignment for nucleotide sequences. *Bioinformatics* **34(18)**, 3094–3100 (2018).

Li, W. & Godzik, A. Cd-hit: a fast program for clustering and comparing large sets of protein or nucleotide sequences. *Bioinformatics* **22(13)**, 1658–1659 (2006).

Lupas, A., Van Dyke, M. & Stock, J. Predicting coiled coils from protein sequences. *Science* **252**, 1162–1164 (1991).

Love, M. I., Huber, W. & Anders, S. Moderated estimation of fold change and dispersion for RNA-seq data with DESeq2. *Genome Biol* **15**, 550 (2014).

Kim, D., Langmead, B. & Salzberg, S. L. HISAT: a fast spliced aligner with low memory requirements. *Nat. Methods* **12**, 357–360 (2015).

Marçais, G. *et al*. MUMmer4: a fast and versatile genome alignment system. *PLoS Comput. Biol.* **14**, e1005944 (2018).

Massonnet, M. *et al*. The genetic basis of sex determination in grapes. *Nat Commun* **11**, 2902 (2020).

McHale, L., Tan, X., Koehl, P. & Michelmore, R. W. Plant NBS-LRR proteins: adaptable guards. *Genome Biol* **7**, 212 (2006).

McKenna, A. *et al*. The Genome Analysis Toolkit: A MapReduce framework for analyzing next-generation DNA sequencing data. *Genome Res.* **20(9)**, 1297–1303 (2010).

Meyers, B. C. *et al*. Plant disease resistance genes encode members of an ancient and diverse protein family within the nucleotide binding superfamily. *Plant J* **20**, 317–332 (1999).

Michelmore, R. W., Christopoulou, M. & Caldwell, K. S. Impacts of resistance gene genetics, function, and evolution on a durable future. *Annu Rev Phytopathol.* **51**, 291–319 (2013).

Miedes, E., Vanholme, R., Boerjan, W. & Molina, A. The role of the secondary cell wall in plant resistance to pathogens. *Front Plant Sci.* **5**, 358 (2014).

Patro, R., Duggal, G., Love, M. I., Irizarry, R. A. & Kingsford, C. Salmon provides fast and bias-aware quantification of transcript expression. *Nat Methods* **14(4)**, 417–419 (2017).

Prigozhin, D. M. & Krasileva, K. V. Analysis of intraspecies diversity reveals a subset of highly variable plant immune receptors and predicts their binding sites. *Plant Cell* **33(4)**, 998–1015 (2021).

Olmo, H. P. *Vinifera rotundifolia* hybrids as wine grapes. *Am. J. Enol. Vitic.* **22**, 87–91 (1971).

Olmo, H. P. The potential role of (*vinifera* x *rotundifolia*) hybrids in grape variety improvement. *Experientia* **42**, 921–926 (1986).

Pap, D. *et al*. Identification of two novel powdery mildew resistance loci, *Ren6* and *Ren7*, from the wild Chinese grape species *Vitis piasezkii*. *BMC Plant Biol.* **16**, 170 (2016).

Pauquet, J. *et al*. Establishment of a local map of AFLP markers around the powdery mildew resistance gene *Run1* in grapevine and assessment of their usefulness for marker assisted selection. *Theor Appl Genet* **103**, 1201–1210 (2001).

Qiu, W., Feechan, A. & Dry, I. Current understanding of grapevine defense mechanisms against the biotrophic fungus (*Erysiphe necator*), the causal agent of powdery mildew disease. *Hortic Res* **2**, 15020 (2015).

Quinlan, A. R. BEDTools: the Swiss-army tool for genome feature analysis. *Curr Protoc Bioinformatics* **47**, 11.12.1-34 (2014).

Ramming, D. W. *et al*. A single dominant locus, *Ren4*, confers rapid non-race-specific resistance to grapevine powdery mildew. *Phytopathology* **101**, 502-508 (2011).

Reifschneider, F. J. & Boiteux, L. S. A vacuum-operated settling tower for inoculation of powdery mildew fungi. *Phytopathology* **78**, 1463–1465 (1988).

Riaz, S., Tenscher, A. C., Ramming, D. W. & Walker, M. A. Using a limited mapping strategy to identify major QTLs for resistance to grapevine powdery mildew (*Erysiphe necator*) and their use in marker-assisted breeding. *Theor Appl Genet* **122**, 1059–1073 (2011).

Riaz, S. *et al*. Identification of mildew resistance in wild and cultivated Central Asian grape germplasm. *BMC Plant Biol* **13**, 149 (2013).

Riaz, S., Menéndez, C. M., Tenscher, A., Pap, D. & Walker, M. A. Genetic mapping and survey of powdery mildew resistance in the wild Central Asian ancestor of cultivated grapevines in Central Asia. *Hort Res* **7**, 104 (2020).

Robinson, J. T. *et al*. Integrative genomics viewer. *Nat. Biotechnol.* **29**, 24–26 (2011).

Saitou, N. & Nei, M. The neighbor-joining method: A new method for reconstructing phylogenetic trees. *Mol. Biol. Evol.* **4**, 406–425 (1987).

Sambucci, O., Alston, J. M., Fuller, K. B. & Lusk, J. The pecuniary and non-pecuniary costs of powdery mildew, and the potential value of resistant varieties in California grapes. *Am J Enol Vitic* **70(2)**, 177–187 (2019).

Seo, E., Kim, S., Yeom, S. I. & Choi, D. Genome-wide comparative analyses reveal the dynamic evolution of nucleotide-binding leucine-rich repeat gene family among Solanaceae plants. *Front Plant Sci*. **7**, 1205 (2016).

Shen, W., Le, S., Li, Y. & Hu, F. SeqKit: A Cross-Platform and Ultrafast Toolkit for FASTA/Q File Manipulation. *PloS One* **11(10)**, e0163962 (2016).

Small, J. K. (eds) Flora of the southeastern United States: being descriptions of the seed-plants, ferns and fern-allies growing naturally in North Carolina, South Carolina, Georgia, Florida, Tennessee, Alabama, Mississippi, Arkansas, Louisiana and in Oklahoma and Texas east of the one hundredth meridian. (J.K. Small, 1913).

Soneson, C., Love, M. I. & Robinson, M. D. Differential analyses for RNA-seq: transcript-level estimates improve gene-level inferences. *F1000Res.* **4**, 1521 (2015).

Steuernagel, B. K. *et al*. The NLR-Annotator tool enables annotation of the intracellular immune receptor repertoire. *Plant Physiol.* **183**, 468–482 (2020).

Suzuki, N. *et al*. Respiratory burst oxidases: the engines of ROS signaling. *Curr Opin Plant Biol.* **14(6)**, 691–699 (2011).

Trapnell, C. *et al*. Transcript assembly and abundance estimation from RNA-Seq reveals thousands of new transcripts and switching among isoforms. *Nature Biotechnol.* **28(5)**, 511–515 (2010).

Xiao, S. *et al*. Broad spectrum mildew resistance in *Arabidopsis thaliana* mediated by RPW8. *Science* **291**, 118–120 (2001).

Zhao, Q. *et al*. Laccase is necessary and nonredundant with peroxidase for lignin polymerization during vascular development in *Arabidopsis*. *Plant Cell* **25**, 3976–3987 (2013).

Zuckerkandl, E. & Pauling, L. Evolutionary divergence and convergence in proteins. In Evolving Genes and Proteins (eds Bryson, V. & Vogel, H. J.) 97–166 (Academic Press, 1965).

Zyprian, E. *et al*. Quantitative trait loci affecting pathogen resistance and ripening of grapevines. *Mol Genet Genomics* **291**, 1573–1594 (2016).